Nondipole effects in helium ionization by intense soft x-ray laser pulses

Henri Bachau, Matabara Dieng

EPJ manuscript No.
(will be inserted by the editor)

Nondipole effects in helium ionization by intense soft x-ray laser pulses

Henri Bachau[1] and Matabara Dieng[2]

[1] Centre des Lasers Intenses et Applications (CELIA, UMR5107 du CNRS-CEA-Université de Bordeaux), 351 Cours de la Libération, 33405 Talence Cedex, France, e-mail: henri.bachau@u-bordeaux.fr

[2] Unité de Formation et de Recherche Sciences Appliquées et Technologies de l'Information et de la Communication (SATIC), Université Alioune DIOP de Bambey, B.P. 30, Bambey (Diourbel), Senegal, e-mail: topdigne@yahoo.fr

Received: date / Revised version: date

Abstract. We consider the helium atom exposed to laser pulses in soft-x regime at intensities of the order of $10^{17} - 10^{20}$ W/cm^2. Two cases are investigated, first a pulse with a central frequency of 20 a.u. ($\sim$ 544.2 eV) and a pulse with a central frequeny of 50 a.u. ($\sim$ 1.36 keV). We solve the time-dependent Schrödinger equation (TDSE), nondipole (retardation) effects are included up to $\mathcal{O}(1/c)$ (c being the velocity of light). We study the single photoionization of helium with a focus on nondipole effects. We calculate the total and partial photoelectron energy spectra, and the photoelectron angular distributions. The nondipole effects associated with the $\mathbf{A}\cdot\mathbf{P}$ and $\mathbf{A}^2$ coupling terms in the Hamiltonian ($\mathbf{A}$ denoting the vector potential of the field and $\mathbf{P}$ the momentum operator) are thoroughly analyzed in the region of one-photon resonance. We show that the nondipole contribution associated with $\mathbf{A}\cdot\mathbf{P}$ varies linearly with the intensity I while a three-photon transition involving $\mathbf{A}^2$ increases like I^3, in agreement with lowest order perturbation theory (LOPT). At high intensities these contributions compete and the nondipole transition becomes nonlinear. The physical mechanisms associated with nondipole couplings are discussed, as well as their effects on photoelectron energy and angular distributions.

PACS. PACS-key describing text of that key – PACS-key describing text of that key

1 Introduction

The advent of free electron lasers delivering x-rays at high intensity [1,2] opens the way to the exploration of new regimes in physics, chemistry and bio-imaging. In atomic physics multiphoton processes have been identified in neon in soft x-ray regime at intensities of the order of 10^{17}-10^{18} W/cm^2 [3,4] (LCLS facility, USA) and in xenon above 5 keV at SACLA facility (Japan) [5]. High intensities are also obtained in the hard x-ray regime, to cite a recent application in atomic physics multiphoton multiple ionization of a high-Z atom has been reported at ultra-intense intensity (10^{19} W/cm^2) and photon energies from 5.5 to 8.3 keV [6]. Many FEL sources are now in operation, upgrade or in construction throughout the world, their status as well as the scientific achievements are reported in recent reviews [7–9], the latter focusing more on technology and physics of FELs. Concerning now the target, light atoms, like hydrogen or helium, are ideal candidates to investigate the general mechanisms governing their interaction with light since they are accessible to an accurate theoretical description. But, due to the small photoionization cross section, the x-ray photoelectrons are hardly detectable. Nevertheless, it must be noticed that bright-enough synchrotron sources allows now to study light atoms using x-ray photoelectron spectroscopy [10], and multiphoton processes have been detected in helium at photon energies of 42.8 and 38.4 eV at the FEL facility FLASH (Germany) [11]. FELs operating at high intensities open the way to pursue these investigations in x-ray regime.

In the field of photoelectron spectroscopy of atoms at short wavelengths, observation of nondipole effects in photoelectron angular distributions (PAD) were made in the late 1920s [12] in the hard x-ray photon energy range, while the first experimental studies below 5 keV date back to the late 1960s-early 1970 [13,14]. Thanks to the unique properties of the photons generated by synchrotron facilities, it has been possible to measure nondipole parameters in x-ray regime (like for example the nondipolar asymmetry parameters of PADs in Ar [15]), a tremendous amount of work has been devoted to this field these last fifty years. Due to the relatively low photon fluence at these facilities the theoretical work has been developed in the framework of LOPT. The nondipole corrections are associated with the coupling terms $\mathbf{A}\cdot\mathbf{P}$ and $\mathbf{A}^2$ (diamagnetic term) in the Hamiltonian. In dipole approximation (DA) $\mathbf{A}^2$ does not contribute to light-matter dynamics while the coupling term $\mathbf{A}\cdot\mathbf{P}$ reduces to an electric-dipole (E1) transition. Beyond the DA the correction term $\mathbf{A}^2$, associated with a two-photon transition, can be neglected in the context of the early experiments above cited, the photoionization process involves one-photon absorption and it is dominated by the coupling term $\mathbf{A}\cdot\mathbf{P}$. Using nonrelativistic, independent-particle wavefunctions and developing $\mathbf{A}\cdot\mathbf{P}$ in first-order Cooper [16,17] (see references therein and the Errata [18]) proposed a simple parametrization of the differential cross section, in the form

$$\frac{d\sigma_{nl}}{d\Omega} = \frac{\sigma_{nl}}{4\pi}[1+\beta P_2(\cos\theta)+(\delta+\gamma\cos^2\theta)\sin\theta\cos\phi] \quad (1)$$

for linearly polarized light. In this expression, θ is the angle between the polarization vector and the electron mo-

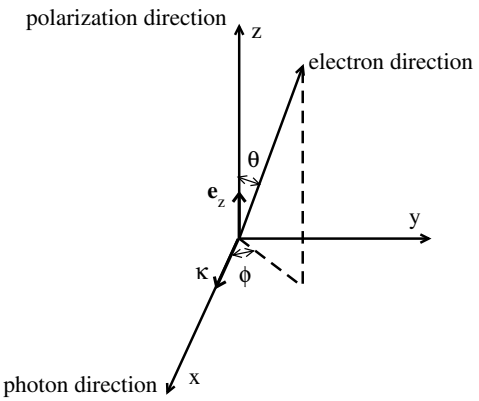

Fig. 1. Definition of the angles θ and ϕ relative to photon, electron and polarization directions, taking the z-axis (unit vector $\mathbf{e}_z$) along the polarization vector and the wavevector κ along $\mathbf{e}_x$ (unit vector of x-axis).

mentum and ϕ is the azimuthal angle, see Fig. 1. σ_{nl} is the angle-integrated cross section, β characterizes the pure electric-dipole (E1) anisotropic parameter while γ and δ are first-order nondipole angular distribution parameters.

Experimental results obtained around FELs at high intensity stimulate the development of theoretical approaches able to describe nonlinear processes with intense and short x-ray pulse. These studies raise the problem of the effects of the retardation terms, with in particular the role of $\mathbf{A}^2$. In this context two-photon ionization processes, like above-threshold ionization in x-ray regime, have been investigated within LOPT [19–21]. Non-perturbative methods have been also developed to investigate the relative contributions of $\mathbf{A}\cdot\mathbf{P}$ and $\mathbf{A}^2$ in one- and two-photon ionization of hydrogen. For example in [22] photons energies ranging from 200 eV to 3 keV have been considered, at the atomic unit of intensity, i.e., $I_0 = 3.51\times10^{16}$ W/cm^2. The conclusion of this study is that, if the contribution of $\mathbf{A}^2$ is non-negligible, the nondipole correction mainly comes from the term $\mathbf{A}\cdot\mathbf{P}$. Incidentally, we notice that the nondipole diamagnetic term $\mathbf{A}^2$ plays a crucial role in nonlinear processes like stimulated Compton Scattering [23] and stimulated Raman Scattering [24]. Analytical approaches, theory and methodologies of the TDSE in the framework of *ab initio* calculations, with a particular focus on dynamical effects induced by the $\mathbf{A}^2$ term, can be found in [25–30]. Here it is worth recalling that, even at intensities of the order of I_0, LOPT applies in x-ray regime since the ponderomotive energy U_p ($U_p = I/4\omega^2$ where I is the intensity and ω the photon energy) is much smaller than the photon energy. At the same time the value of the Keldysh parameter [31], given by $\sqrt{I_p/2U_p}$ (where I_p is the atomic ionization potential) is much greater than 1, unfavorable for tunnel ionization. As a matter of fact, as the intensity increases beyond I_0 and/or the photon energy decreases from x-ray to xuv domain the validity of LOPT and DA must be carefully checked.

A recent theoretical study [30] of the breakdown of DA in the ionization of hydrogen by intense soft x-ray laser pulses (with a photon energy of 50 a.u.) shows that the diamagnetic term $\mathbf{A}^2$ dominates the correction to DA for electric field strengths beyond $E_0 \simeq 100$ a.u., corresponding to an intensity of 3.51×10^{20} W/cm^2. Clearly, the relative importance of the two nondipole correction terms calculated at $I_0 = 3.51\times10^{16}$ W/cm^2 [22] cannot be extrapolated at much higher intensities. Here we investigate the photoionization of helium and nondipole effects

in transitional regime in the intensity range $10^{17} - 10^{20}$ W/cm^2, and photon energies of 544.2 eV (20 a.u.) and 1.36 keV (50 a.u.). Energy and angular distributions are obtained by integrating numerically the TDSE. We focus on one-photon resonance region, calculations are performed in DA and including the nondipole corrections associated with the coupling terms $\mathbf{A}\cdot\mathbf{P}$ and $\mathbf{A}^2$ up to $\mathcal{O}(1/c)$. The effects and relative importance of the nondipole terms are discussed, as well as the physical processes underlying the associated transitions.

Atomic units (a.u.) are used throughout this paper unless otherwise stated.

2 Theory

In this section we refer to the nonperturbative (TDSE) approach. We follow the numerical method previously developed in [22]. We recall only the main steps.

We start from the well-known expression of the nonrelativistic Hamiltonian operator for a one-active electron atom in an external electromagnetic field of vector potential $\mathbf{A}$ (in the Coulomb gauge):

$$\mathcal{H} = \frac{1}{2}[\mathbf{P} + \mathbf{A}(\mathbf{r},t)]^2 + V(r). \tag{2}$$

The atomic potential $V(r)$ is a central one, it has the form

$$V(r) = -\frac{1}{r} - \frac{1}{r}(1+\lambda r)e^{-2\lambda r}. \tag{3}$$

This potential is widely used in atomic and molecular physics (see [35] and references therein). It verifies the correct asymptotic conditions for He; $V(r) \underset{r\to 0}{\sim} -2/r$ and $V(r) \underset{r\to\infty}{\sim} -1/r$. Here $\lambda = 1.688$, this parameter is chosen such that the absolute value of the lowest eigenenergy (here associated with the $1s$ state of the model atom) of the field free Hamiltonian reproduces the ionization potential of helium (~ 0.9037 a.u.). Taking the z-axis (unit vector $\mathbf{e}_z$) along the polarization vector and the wavevector κ along $\mathbf{e}_x$ (unit vector of x-axis) as shown in Fig. 1, the vector potential reads;

$$\mathbf{A}(\mathbf{r},t) = A(t-\alpha x)\,\mathbf{e}_z \tag{4}$$

with α the fine structure constant ($\alpha = 1/c$). Considering that $\alpha\,\omega \leq 1$ (or $\omega \leq 3.73$ keV) $A(t-\alpha x)$ is approximated by its truncated power series in x. Keeping only the first-order correction in α one can show that the Hamiltonian can be written

$$\mathcal{H} \approx H_a + \mathcal{H}^{(1)}_{DA} + \mathcal{H}^{(1)}_{RET} + \mathcal{H}^{(2)}_{RET}. \tag{5}$$

It is expressed as a sum of the atomic Hamiltonian $H_a \equiv \mathbf{P}^2/2 + V(r)$, of the interaction term in DA

$$\mathcal{H}^{(1)}_{DA} = A(t)\,P_z, \tag{6}$$

and of two other terms, describing nondipole corrections;

$$\mathcal{H}^{(1)}_{RET} = \alpha\,F(t)\,x\,P_z \tag{7}$$

and

$$\mathcal{H}^{(2)}_{RET} = \alpha\,F(t)\,A(t)\,x \tag{8}$$

where $F(t) = -\dot{A}(t)$. Within first-order perturbation theory, the terms $\mathbf{A}\cdot\mathbf{P} \equiv \mathcal{H}^{(1)}_{DA} + \mathcal{H}^{(1)}_{RET}$ and $\mathbf{A}^2 \equiv \mathcal{H}^{(2)}_{RET}$ induce one and two-photon transitions, respectively. The selection rule is ($\Delta l = \pm 1; \Delta m = 0$) in DA (term $\mathcal{H}^{(1)}_{DA}$) and for nondipole coupling terms ($\Delta l = 0, \pm 2; \Delta m = \pm 1$) for $\mathcal{H}^{(1)}_{RET}$ and ($\Delta l = \pm 1; \Delta m = \pm 1$) for $\mathcal{H}^{(2)}_{RET}$.

The TDSE reads

$$i\frac{\partial}{\partial t}\psi(\mathbf{r},t) = \widetilde{\mathcal{H}}\psi(\mathbf{r},t). \tag{9}$$

The above equation is resolved by using four different approximations for the Hamiltonian $\widetilde{\mathcal{H}}$. First we consider the DA with $\widetilde{\mathcal{H}} \equiv H_a + \mathcal{H}^{(1)}_{DA}$ (see Eq. 5). Second we consider the Hamiltonian $\widetilde{\mathcal{H}} \equiv H_a + \mathcal{H}^{(1)}_{DA} + \mathcal{H}^{(1)}_{RET}$ which (only) includes the contributions associated with the coupling term $\mathbf{A}\cdot\mathbf{P}$. Then we use $\widetilde{\mathcal{H}} \equiv H_a + \mathcal{H}^{(1)}_{DA} + \mathcal{H}^{(2)}_{RET}$ where the nondipole correction associated with $\mathbf{A^2}$ is added to the coupling term $\mathbf{A}\cdot\mathbf{P}$ in DA ($\mathcal{H}^{(1)}_{DA}$). Finally the full expression (5) is considered; $\widetilde{\mathcal{H}} \equiv H_a + \mathcal{H}^{(1)}_{DA} + \mathcal{H}^{(1)}_{RET} + \mathcal{H}^{(2)}_{RET}$. These four approaches allow to evaluate the relative contributions of DA and nondipole coupling terms. In the following they will be referred to as TDSE-DA, TDSE-AP, TDSE-DA-A^2 and TDSE-FULL, respectively.

A spectral method is used to resolve the TDSE. First, we define the amplitude $A(t)$ of the field vector potential such that it is non-zero over the time interval ($-T/2$,$T/2$) where T is the total pulse duration (i.e., the full extension of the pulse support), $A(t)$ is chosen to have a $\cos^2$ envelope. Under these conditions the laser bandwidth, defined as the FWHM of the square of the Fourier transform of the field amplitude, is given by $1.44\times 2\pi/T$. As mentioned above the laser field is linearly polarized along the z-axis. In order to calculate the time-dependent wave function $\psi(\mathbf{r},t)$, solution of the TDSE, we use the expansion

$$\psi(\mathbf{r},t) = \sum_{n,\,l,\,m} e^{-iE_{nl}t}\, c^{(l,m)}_n(t)\, u_{nlm}(\mathbf{r}) \tag{10}$$

in a discrete basis of H_a eigenfunctions

$$u_{nlm}(\mathbf{r}) = X_{nl}(r)/r\, Y_{lm}(\mathbf{r}/r). \tag{11}$$

The eigenvalues of H_a, indexed as E_{nl}, are determined together with the radial eigenfunctions $X_{nl}(r)$ by solving numerically the radial Schrödinger equation in a basis of B-spline functions [36]. The coupled differential equations satisfied by the coefficients $c^{(l,m)}_n(t)$ are integrated from $t=-T/2$ to $t=T/2$ using an explicit time-adaptive Runge-Kutta method, with initial conditions (at $t=-T/2$) corresponding to He in its ground state, i.e., here the $1s$ state. In a typical calculation we use angular momenta $l=0-10$, with $|m|\le l$, and a basis of 2500 B-spline functions of order $k=7$, distributed linearly inside a box of length $b=600$ a.u. for the case $\omega=20$ a.u. and $b=300$ a.u. for $\omega=50$ a.u. The box radius b is chosen such that the probability to find the photoelectron outside the box at the end of the pulse is negligible. The convergence of the calculations is checked by varying the box size and/or the number of basis functions and angular momenta, we will return to this point later.

Once the wave function $\psi(\mathbf{r},t)$ is known at the end of the pulse, the angle-integrated photoelectron energy spectrum (PES) and PADs can be extracted from it. Partial photoelectron energy spectrum (PPS), associated with channels of given l' and m' can be also extracted, in the following they will be referred to as PPS ($l=l', m=m'$). As we will see below, the PPSs associated with the different approximations of $\widetilde{\mathcal{H}}$ allow to identify and to quantify the effects of nondipole coupling terms, as well as the contribution in DA. The procedure used to extract the angular distributions is presented in the appendix of [22], we do not repeat it here. The only difference with [22] is that the

eigenfunctions of the field free Hamiltonian H_a are not hydrogenic ones, since $V(r)$ is not a pure Coulomb potential. In the context of TDSE, this has not a major impact on calculations (for the extraction of angular distributions a phase shift must be calculated for each angular momentum l in addition to the Coulomb one). Nevertheless it is worth noticing that the presence of a screened Coulomb potential has a major impact in the context of perturbation theory (PT) since analytic approaches, valid in the case of hydrogenic systems (see [20, 21] and references therein), cannot be used.

Before presenting the results we briefly discuss the limitations of the one-active electron model. It only represents singly excited (and ionized) states of He and not the doubly-excited states and ionization-excitation. The latter channels are energetically open here, through Raman-type processes or direct photon absorption. First we note that the photoionization of He is dominated by the channel leaving the He^+ ion in $1s$ state at the wavelengths considered here [32]. Given the laser bandwidths (about 0.18 a.u. for the case of frequency $\omega = 20$ a.u. and 0.33 a.u. for $\omega = 50$ a.u.) the ionization-excitation channels should lead to structures in the electron spectrum well separated in energy from the main photoionization peak. Regarding now the excitation of bound states of He it relies on stimulated Raman scattering, we have demonstrated in previous work [24] that the dominant contribution is associated with the diamagnetic term $\mathcal{H}^{(2)}_{RET}$ in first order of PT, it populates the $1snp$ series with $m = \pm 1$. The other contribution is associated with the DA term $\mathcal{H}^{(1)}_{DA}$ in second-order of PT, leading to the population of $1sns$ and $1snd$ series with $m = 0$ ($1sns$ dominating over $1snd$). In this context the contribution of $\mathcal{H}^{(1)}_{RET}$ is negligible. We have checked that these trends hold in this work. Similar processes could populate doubly excited series as well the associated ionization-excitation channels in the low energy continuum. This is an interesting subject in itself but due to the laser bandwidths considered here, which are much smaller than the He ionization threshold, these transitions are not expected to play a significant role. A two-color scheme [23] should be more appropriate to study electronic double excitation. Incidentally we mention that the selection rules given above for DA and nondipole correction terms are strictly valid for the one-active electron model (see [33] and [34] for the rules in DA and retardation couplings in the general case).

3 Results

3.1 Laser pulse central frequency of 20 a.u. (~ 544.2 eV)

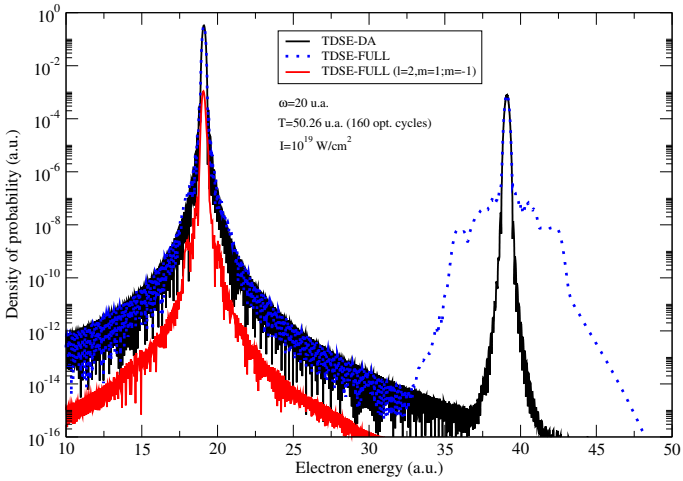

Fig. 3. PESs calculated in DA (TDSE-DA) and with full Hamiltonian (TDSE-FULL). PPS ($l = 2, m = 1; m = -1$) (sum of the PPS ($l = 2, m = 1$) and PPS ($l = 2, m = -1$)) calculated with TDSE-FULL. The central frequency $\omega = 20$ a.u., the pulse duration $T \approx 50.26$ a.u. and the intensity $I = 10^{19}$ W/cm^2.

We consider the case of a pulse with central photon energy $\omega = 20$ a.u. and total pulse duration of 160 optical cycles ($T = \frac{320\pi}{\omega} \approx 50.26$ a.u.). In Fig. 2 we present the PESs at intensities of 10^{17}, 10^{18} and 10^{19} W/cm^2, calculations are performed in DA (TDSE-DA). The figure shows two peaks at energies close to 19.1 a.u. (peak 1) and 39.1 a.u. (peak 2), corresponding to one- and two-photon absorption, respectively. In DA the peak 1 has a component ($l = 1, m = 0$) and the peak 2 is the addition of the PPSs ($l = 0, m = 0$) and ($l = 2, m = 0$), the others channels are negligible. The probability density increases linearly with the intensity in the region of peak 1 while it increases quadratically in the region of peak 2, in agreement with LOPT. We have checked that a very good agreement is found for the one-photon tran-

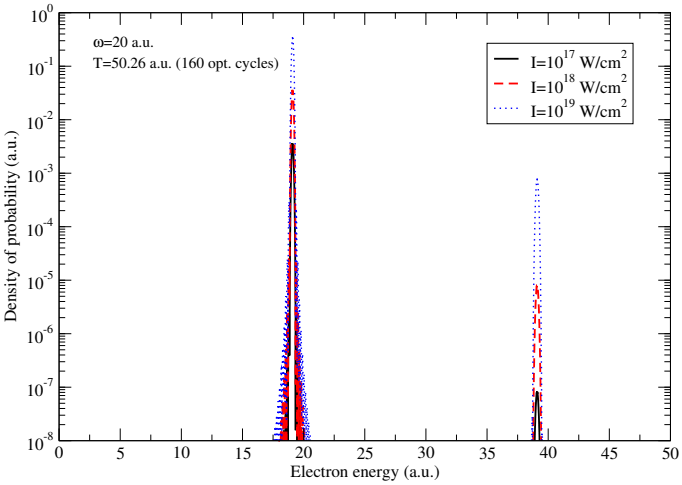

Fig. 2. PES in DA, calculated at various intensities (see the inset). The central frequency $\omega = 20$ a.u. and the pulse duration $T \approx 50.26$ a.u.

sition with a time-dependent PT calculation. We present in Fig. 3 TDSE-DA and TDSE-FULL calculations at the intensity $I = 10^{19}$ W/cm^2. The figure shows the dominant nondipole contribution for peak 1, it is the PPS ($l = 2, m = \pm 1$). For symmetry reasons the PPSs ($l = 2, m = 1$) and ($l = 2, m = -1$) are similar, the PPS ($l = 2, m = 1; m = -1$) (see the inset in Fig. 3) is the sum of the two. First the figure clearly shows that the DA contribution, in the region of peak 1, is three orders of magnitude larger than the nondipole one, the latter being of the order of magnitude of peak 2. As a consequence the TDSE-DA and TDSE-FULL curves overlap. Nevertheless the TDSE-FULL curve broadens irregularly at the wings of both peaks (this appears more clearly at peak 2 in Fig. 3). This broadening is due to the slow numerical convergence of the TDSE-FULL calculations with l in expansion (10).

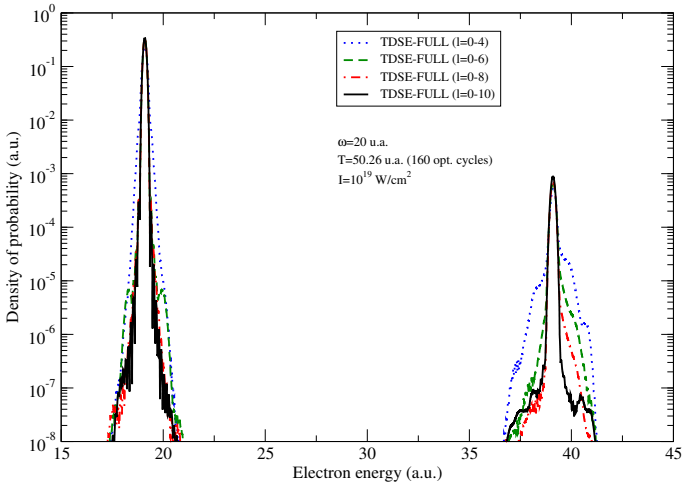

Fig. 4. PES calculated with various basis set expansion in l (see the inset). The laser parameters are the same as in Fig. 3.

We present in Fig. 4 TDSE-FULL calculations at $I = 10^{19}$ W/cm^2 performed with four different basis sets; $l = 0 - l_{max}$ with $l_{max} = 4, 6, 8, 10$. The figure shows the convergence of the calculations as l_{max} increases, for example for peak 1 the curves for $l = 0 - 8$ and $l = 0 - 10$ overlap over a density probability range of four order of magnitude, i.e., about $0.3 - 10^{-5}$ a.u. A similar trend is observed for the PPS ($l = 2, m = \pm 1$) (nondipole contribution, not shown in the figure). Therefore, even if the channels with $l = 1, 2$ dominate at the end of the pulse (at $t = T/2$) in the region of peaks 1, the integration of the TDSE-FULL requires a much larger number of angular momenta l. As expected, higher is the intensity, larger is the value of l_{max} required to reach the numerical convergence of the calculations [29]. Considering that $-l \leq m \leq l$ this rapidly leads to an important increase of the basis set and a dramatic growth of the computational demand.

In the following we focus on the region of peak 1, where the PPS ($l = 2, m = \pm 1$) dominates over the others nondipole channels. In Fig. 5 we present the PPS ($l = 2, m = 1$) for TDSE-FULL, TDSE-DA-A^2 and TDSE-AP calculations, as defined below the Eq. (9). First the right figure shows results for $I = 10^{18}$ W/cm^2, we clearly see that the main contributions to the nondipole effect is related to the coupling term $\mathbf{A} \cdot \mathbf{P}$ (included in TDSE-AP) while the contribution of $\mathbf{A}^2$ (included in TDSE-DA-A^2) is several orders of magnitude smaller. We recall that the selection rule for the term $\mathcal{H}^{(1)}_{RET}$ is ($\Delta l = 0, \pm 2; \Delta m = 1$), thus the PPS ($l = 2, m = 1$) is mainly due the term $\mathcal{H}^{(1)}_{RET}$ which populates this channel through one-photon absorp-

tion from $1s$. The situation is quite different at $I = 10^{19}$ W/cm^2 (left figure). Now the contributions of TDSE-DA-A^2 and TDSE-AP are of the same order of magnitude. The TDSE-AP contribution has increased linearly with the intensity I, in agreement with the one-photon absorption scheme explained above. In parallel with the resolution of the TDSE-AP we have performed time-dependent calculations where $\mathcal{H}^{(1)}_{RET}$ is treated in first-order PT, they are in good agreement with the TDSE-AP PPS ($l = 2, m = 1$) for both intensities, this confirms that it is a one-photon transition in the perturbative regime. If we consider now the TDSE-DA-A^2 contribution, we have identified two pathways involving one- and two-photon resonances. First a one-photon dipole coupling from $1s$ to the channel ($l = 1, m = 0$), followed by a Compton-like two-photon transition from the channel ($l = 1, m = 0$) to the PPS ($l = 2, m = \pm 1$) around the one-photon resonance (at energy $\sim$ 19.1 a.u.). The latter transition is induced by the nondipole coupling term $\mathcal{H}^{(2)}_{RET}$ (associated with $\mathbf{A}^2$) according to the selection rule ($\Delta l = \pm 1; \Delta m \pm 1$), it is a two-photon absorption-emission process. The second process relies on a direct two-photon coupling (through $\mathcal{H}^{(2)}_{RET}$) from $1s$ to the channel ($l = 1, m = \pm 1$) at energy $\sim$ 39.1 a.u., followed by a dipole transition to the channel ($l = 2, m = \pm 1$) at energy $\sim$ 19.1 a.u. The TDSE does not allow to discriminate between these two pathways, but the second one involves a continuum-continuum dipole coupling with high energy continua (in the region of peak 1 and peak 2), this type of coupling is usually very small and we can therefore surmise that the first pathway dominates. Both pathways involve three photons (absorption of two photons and one-photon emission), the PPS ($l = 2, m = \pm 1$) population should therefore increases like I^3, if LOPT is valid. A careful analysis of the TDSE-DA-A^2 contributions (at $I = 10^{18}$ W/cm^2 and $I = 10^{19}$ W/cm^2 in Fig. 5) confirms this behavior. Besides the three-photon processes discussed above we mention the possibility of populating the (np, $m = \pm 1$) excited states through the stimulated Raman process evoked at the end of the section 2, followed by the ionization of the latter states to the ($l = 2, m = \pm 1$) continuum. We have checked that the (np, $m = \pm 1$) series is populated at the end of the pulse but with a rather low probability. This is due to the fact that the laser bandwidth (about 0.18 a.u.) is much smaller than the $1s - np$ energy gap ($1s - 2p \approx 0.78$ a.u.). For example at the intensity of $I = 10^{19}$ W/cm^2 the maximum population is found in ($2p$, $m = 1$; $m = -1$) states and it is of the order of $3.3\,10^{-13}$. The populations of the upper states in the Rydberg series decrease rapidly. Furthermore, an efficient ionization of $2p$ would lead to an additional structure at 19.87 a.u., close to the main peak located at 19.1 a.u., it is clearly absent in figure 4. Finally, it is worth noticing that, at $I = 10^{19}$ W/cm^2, the population of the $1s$ state is close to 0.94 at the end of the pulse, we are therefore close to the limit of validity of PT for the pulse parameters considered.

At contrast with the electron energy distributions the PADs are much more sensitive to nondipole corrections. We show in Fig. 6 the angular distributions versus the azimuthal angle ϕ (see Fig. 1) for two intensities, $I = 10^{18}$

W/cm^2 and $I = 10^{19}$ W/cm^2. These distributions are obtained for the peak 1 by integrating in energy the triply differential distribution (in angles and energy) from 18.0 a.u. to 20.0 a.u. The polar angle θ is fixed at $\pi/4$. The distribution for $I = 10^{18}$ W/cm^2 has been scaled such that the DA distributions for $I = 10^{18}$ W/cm^2 and $I = 10^{19}$ W/cm^2 match. We reconsider now the angular distribution expressed in Eq. (1). We have noticed in the introduction that it takes into account only the $\mathbf{A}\cdot\mathbf{P}$ coupling term in first-order. For a one-electron $s-p$ transition $\beta = 2$ and $\delta = 0$ [17], therefore the PAD differential probability reads

$$\frac{dP_{1s}}{d\Omega} \propto (3\cos^2\theta + \gamma\cos^2\theta\sin\theta\cos\phi). \qquad (12)$$

We recall that γ is the nondipole angular parameter. As expected the DA distribution is flat ($\gamma = 0$ in DA) in Fig. 6, the TDSE-FULL PADs clearly show the influence of the nondipole effects. There is a very good fit to the analytic formula (12) at both intensities, it is obtained with $\gamma \approx 0.51$, in agreement with the value of γ calculated by Amusia et al [37] beyond the framework of one-electron approximation (see Fig. 1 in [37]). It is worth noticing that in [37] electron correlations have been found to be unimportant in the calculation of γ in the case of He $1s$ shell, this explains the agreement between our one-active electron model atom and the above-cited multielectronic approach. We notice the agreement obtained for $I = 10^{19}$ W/cm^2, although the contribution of $\mathbf{A}^2$ is non-negligible at this intensity. In order to check the influence of the latter term we have calculated the PAD with TDSE-DA-A^2 (always integrating the differential distribution over the peak 1, i.e., from 18.0 a.u. to 20.0 a.u.). $\mathbf{A}^2$ has little effect on the angular distribution, the PAD is close to the one obtained in DA. As a consequence the angular distribution is dominated by the $\mathbf{A}\cdot\mathbf{P}$ coupling.

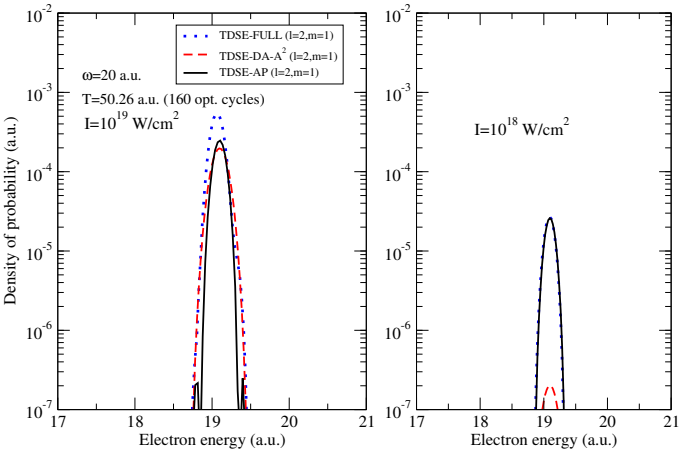

Fig. 5. PPS ($l = 2, m = 1$) calculated with full Hamiltonian (TDSE-FULL) and including the nondipole correction associated with $\mathbf{A}\cdot\mathbf{P}$ (TDSE-AP) and $\mathbf{A}^2$ (TDSE-DA-A^2). The intensity $I = 10^{19}$ W/cm^2 (left figure) and $I = 10^{18}$ W/cm^2 (right figure). The others laser parameters are the same as in Fig. 2.

3.2 Laser pulse central frequency of 50 a.u. ($\sim$ 1.36 keV)

We have performed calculations for $\omega = 50$ a.u., $I = 10^{20}$ W/cm^2, and a pulse duration $T \approx 18.85$ a.u. (150 optical cycles).

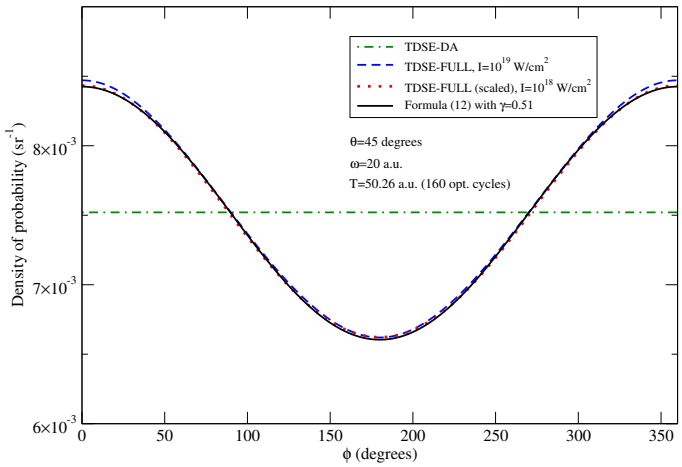

Fig. 6. PAD vs the azimuthal angle ϕ, the polar angle $\theta = 45$ degrees. The intensities are $I = 10^{19}$ W/cm^2 and $I = 10^{18}$ W/cm^2. The others laser parameters are the same as in Fig. 2. For $I = 10^{18}$ W/cm^2 the angular distribution has been scaled such that the angular distributions in DA match for both intensities. The figure also shows the angular distribution calculated with the formula (12), with $\gamma = 0.51$.

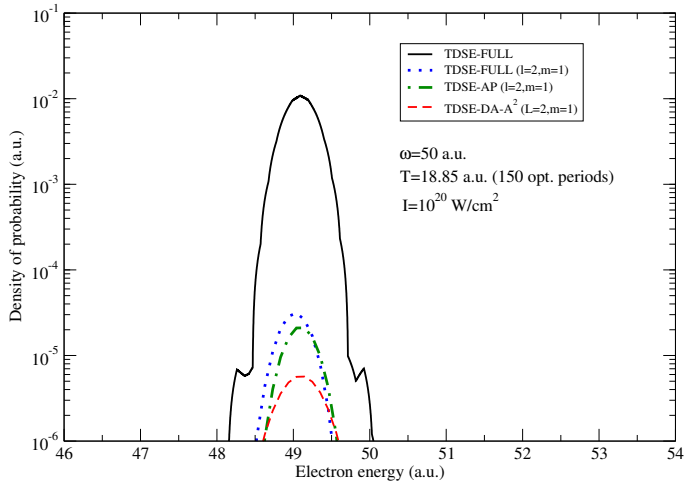

Fig. 7. PES and PPS ($l = 2, m = 1$) calculated with the full Hamiltonian (TDSE-FULL). PPSs ($l = 2, m = 1$) are also calculated considering nondipole correction associated with $\mathbf{A} \cdot \mathbf{P}$ (TDSE-AP) and $\mathbf{A}^2$ (TDSE-DA-A^2). The central frequency $\omega = 50$ a.u., the pulse duration $T \approx 18.85$ and the intensity $I = 10^{20}$ W/cm^2.

The Fig. 7 shows the PES associated with the full Hamiltonian (TDSE-FULL) as well as the PPSs ($l = 2, m = 1$) calculated by using TDSE-FULL, TDSE-AP and TDSE-DA-A^2. As in the case of $\omega = 20$ a.u., the leading nondipole correction is the PPS ($l = 2, m = \pm 1$). It is at its maximum three orders of magnitude lower than the DA contribution and of the order of magnitude of the peak associated with two-photon absorption (not shown in the figure). The nondipole correction associated with the coupling term $\mathbf{A} \cdot \mathbf{P}$ dominates, it is about four times larger than the contribution of $\mathbf{A}^2$ (see the curves TDSE-AP and TDSE-DA-A^2 in Fig. 7). We have checked that, as in the precedent case, the latter correction varies like I^3 while the former one varies linearly with I. LOPT holds for the laser parameters considered. Notice that, at contrast with the case $\omega = 20$ a.u., the population of the $1s$ state is close to 1 at the end of the pulse. Considering the dependence of the nondipole couplings with the intensity I, the nondipole correction $\mathbf{A}^2$ should dominate over the one associated with $\mathbf{A} \cdot \mathbf{P}$ at $I > 10^{20}$ W/cm^2. This agrees with the findings of Moe and Førre [30].

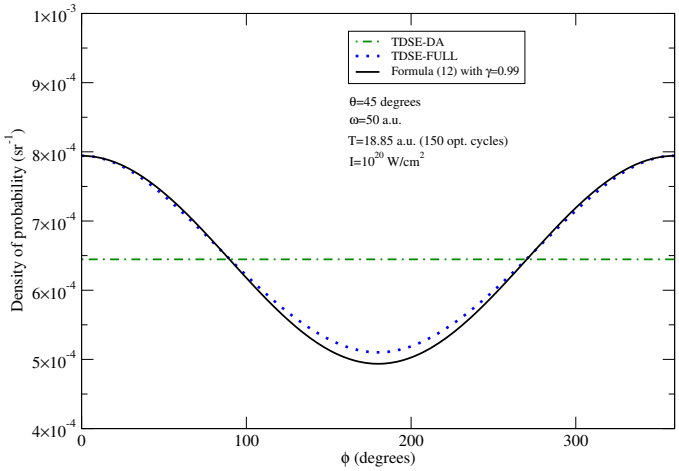

Fig. 8. PAD vs the azimuthal angle ϕ, the polar angle $\theta = 45$ degrees. Laser parameters are the same as in Fig. 7. The angular distributions are calculated in DA (TDSE-DA) and with the full Hamiltonian (TDSE-FULL). The figure also shows the angular distribution calculated with the formula (12), with $\gamma = 0.99$.

The PAD is shown in Fig. 8, as in the precedent case the polar angle is fixed at $\theta = \pi/4$. It is obtained by integrating the triply differential distribution in the region of one-photon resonance, i.e., over the energy range $48-50$ a.u. The PAD fits the analytic formula (12) with $\gamma \approx 0.99$, a value in agreement with the above-mentioned theoretical work [37]. As in the precedent case, the diamagnetic term $\mathbf{A}^2$ has a little impact on the PAD.

4 Conclusions

We have presented a study of nondipole effects in the ionization of helium atom exposed to an intense soft x-ray pulse. First we have considered the case $\omega = 20$ a.u. and pulse duration $T = 50.26$ a.u. (160 optical cycles). For the intensities considered ($I = 10^{17} - 10^{19}$ W/cm^2) the photoionization is dominated by the dipole transition, it populates the channel $(l = 1, m = 0)$ at energies close to 19.1 a.u. Below $I = 10^{19}$ W/cm^2 the dominant nondipole contribution is associated with $\mathbf{A} \cdot \mathbf{P}$ ($\mathcal{H}^{(1)}_{RET}$ in Eq. 5), it is about three orders of magnitude smaller than the dipole contribution and it populates the channel $(l = 2, m = \pm 1)$ through one-photon absorption from $1s$. At the intensity $I = 10^{18}$ W/cm^2, both the dipole and the dominant nondipole transitions increase linearly with the intensity, in agreement with PT. At $I = 10^{19}$ W/cm^2, the nondipole term $\mathbf{A}^2$ comes into play. Combined with a dipole coupling, it populates the channel $(l = 2, m = \pm 1)$ in the region of one-photon resonance (at energy $\sim$ 19.1 a.u.) and it is of the same order of magnitude as the nondipole contribution associated with $\mathbf{A} \cdot \mathbf{P}$. This process is nonlinear, three photons are involved in different combinations where two photons are absorbed and one is emitted. The transition rate varies like I^3, in agreement with LOPT. Regarding now the PAD it fits well the parametrization of Cooper [16,17], based on a first-order treatment of the coupling term $\mathbf{A} \cdot \mathbf{P}$ in PT. The diamagnetic term $\mathbf{A}^2$ does not affect the PAD associated with the energy integrated one-photon resonant peak at the intensities considered. The general trends of the distributions calculated at $\omega = 20$ a.u. are also observed at $\omega = 50$ a.u., but at higher intensities. At $I = 10^{20}$ W/cm^2 and $T = 18.85$ a.u. (150 optical cycles) the nondipole contributions from $\mathbf{A} \cdot \mathbf{P}$ and $\mathbf{A}^2$ are of the same order of magnitude and they vary with the intensity like I and I^3, respectively, in

agreement with LOPT. As in the case of $\omega = 20$ a.u. the PAD fits well the parametrization of Cooper.

In conclusion, studying photoionization at intensities ranging from 10^{17} to 10^{20} W/cm^2, we have identified a transition regime for nondipole effects in the region of one-photon resonance. At the lowest intensities they are dominated by the coupling term $\mathbf{A}\cdot\mathbf{P}$ and the transition rate varies linearly with I, this is the usual situation encountered in synchrotron experiments. As the intensity increases a nonlinear three-photon transition involving the combined effect of one-photon dipole ($\mathcal{H}^{(1)}_{DA}$) and two-photon nondipole ($\mathbf{A}^2$) couplings competes with the linear nondipole contribution associated with $\mathbf{A}\cdot\mathbf{P}$. Both nondipole contributions populate the PPS ($l = 2, m = \pm 1$), with a rate varying like I^3 for the nonlinear one, the ionization rates follow LOPT rules. In all cases, the energy integrated angular distributions are dominated by the coupling term $\mathbf{A}\cdot\mathbf{P}$.

M.D. acknowledges the support for mobility from the University Alioune DIOP of Bambey (Senegal) and is grateful for the hospitality and support from the laboratory CELIA. The TDSE code package used in this work has been developed in a collaboration with M. Dondera (University of Bucharest, Romania) [22], the authors would like to give him the credit for that. H.B. thanks F. Catoire for a careful reading of the manuscript and useful suggestions.

5 Authors contributions

All the authors were involved in the preparation of the manuscript. They have read and approved the final manuscript.

References

1. P. Emma *et al*, Nat. Photon. **4**, 641 (2010)
2. T. Ishikawa *et al*, Nat. Photon. **6**, 540 (2012)
3. L. Young *et al*, Nature (London) **466**, 56 (2010)
4. G. Doumy *et al*, Phys. Rev. Lett. **106**, 083002 (2011)
5. H. Fukuzawa *et al*, Phys. Rev. Lett. **110**, 173005 (2013)
6. B. Rudek *et al*, Nat. Commun. **9**, 4200 (2018)
7. E.A. Seddon *et al*, Rep. Prog. Phys. **80**, 115901 (2017)
8. C. Bostedt *et al*, Rev. Mod. Phys. **88**, 015007 (2016)
9. C. Pellegrini, A. Marinelli, S. Reiche, Rev. Mod. Phys. **88**, 015006 (2016)
10. J-Q. Zhong, M. Wang, W.H. Hoffmann, M.A. van Spronsen, D. Lu, J.A. Boscoboinik, Appl. Phys. Lett. **112**, 091602 (2018)
11. A.A. Sorokin, M. Wellhöfer, S.V. Bobashev, K. Tiedtke, M. Richter, Phys. Rev. A **75**, 051402 (2007)
12. P. Auger, F. Perrin, J. Phys. Radium **8**, 93 (1927)
13. M.O. Krause, Phys. Rev. **177**, 151 (1969)
14. F. Wuilleumier, M.O. Krause, Phys. Rev. A **10**, 242 (1974)
15. B. Krässig, M. Jung, D.S. Gemmell, E.P. Kanter, T. LeBrun, S.H. Southworth, L. Young, Phys. Rev. Lett. **75**, 4736 (1995)
16. J.W. Cooper, Phys. Rev. A **42**, 6942 (1990)
17. J.W. Cooper, Phys. Rev. A **47**, 1841 (1993)
18. J.W. Cooper, Phys. Rev. A **45**, 3362 (1992)
19. H.R. Varma, M.F. Ciappina, N. Rohringer, R. Santra, Phys. Rev. A **80**, 053424 (2009)

20. V. Florescu, O. Budriga, H. Bachau, Phys. Rev. A **84**, 033425 (2011)

21. V. Florescu, O. Budriga, H. Bachau, Phys. Rev. A **86**, 033413 (2012)

22. M. Dondera, H. Bachau, Phys. Rev. A **85**, 013423 (2012)

23. H. Bachau, M. Dondera, V. Florescu, Phys. Rev. Lett. **112**, 073001 (2014)

24. H. Bachau, M. Dondera, Eur. Phys. Lett. **114**, 23001 (2016)

25. M. Førre, S. Selstø, J.P. Hansen, L.B. Madsen, Phys. Rev. Lett. **95**, 043601 (2005)

26. D. Dimitrovski, M. Førre, L.B. Madsen, Phys. Rev. A **80**, 053412 (2009)

27. M. Førre, A.S. Simonsen, Phys. Rev. A **90**, 053411 (2014)

28. A.S. Simonsen, T. Kjellsson, M. Førre, E. Lindroth, S. Selstø, Phys. Rev. A **93**, 053411 (2016)

29. T. Kjellsson, M. Førre, A.S. Simonsen, S. Selstø, E. Lindroth, Phys. Rev. A **96**, 023426 (2017)

30. T.E. Moe, M. Førre, Phys. Rev. A **97**, 013415 (2018)

31. L.V. Keldysh, Sov. Phys. JETP **20**, 1307 (1965)

32. R. Wehlitz *et al*, J. Phys. B: At. Mol. Opt. Phys. 30, L51 (1997)

33. Hans A. Bethe and Edwin E. Salpeter, *Quantum Mechanics of One- and Two-Electron Atoms* (Pluenum/Rosetta Edition, New-York, 1977)

34. B.H. Bransden and C.J. Joachain, *Physics of Atom and Molecules* (Pearson Education, Harlow, 2nd Edition, 2003)

35. H. Bachau, P. Galan, F. Martín, Phys. Rev. A **41**, 3534 (1990)

36. H. Bachau, E. Cormier, P. Decleva, J.E. Hansen, F. Martín, Rep. Prog. Phys. **64**, 1815 (2001)

37. M.Ya. Amusia, A.S. Baltenkov, L.V. Chernysheva, Z. Felfli, A.Z. Msezane, Phys. Rev. A **63**, 052506 (2001)